Japan. S.S. was a research assistant for the Global COE Program for Human Metabolomic Systems Biology.

References

1) Ron D, and Walter P, *Nature Reviews Molecular Cell Biology*, **8**, 519-529 (2007).

2) Zhao L, and Ackerman SL, *Curr Opin Cell Biol*, **18**, 444-452 (2006).

3) DuRose JB, Tam AB, and Niwa M, *Molecular biology of the cell*, **17**, 3095-3107 (2006).

4) Wang XZ, Harding HP, Zhang Y, Jolicoeur EM, Kuroda M, and Ron D, *Embo J*, **17**, 5708-5717 (1998).

5) Pincus D, Chevalier MW, Aragon T, van Anken E, Vidal SE, El-Samad H, and Walter P, *PLoS Biol*, **8**, e1000415 (2010).

6) Bertolotti A, Zhang Y, Hendershot LM, Harding HP, and Ron D, *Nat Cell Biol*, **2**, 326-332 (2000).

7) Shamu CE, and Walter P, *Embo J*, **15**, 3028-3039 (1996).

8) Korennykh AV, Egea PF, Korostelev AA, Finer-Moore J, Zhang C, Shokat KM, Stroud RM, and Walter P, *Nature*, **457**, 687-693 (2009).

9) Calfon M, Zeng H, Urano F, Till JH, Hubbard SR, Harding HP, Clark SG, and Ron D, *Nature*, **415**, 92-96 (2002).

10) Yoshida H, Matsui T, Yamamoto A, Okada T, and Mori K, *Cell*, **107**, 881-891 (2001).

11) Lee AH, Iwakoshi NN, and Glimcher LH, *Mol Cell Biol*, **23**, 7448-7459 (2003).

12) Nagai T, Sawano A, Park ES, and Miyawaki A, *Proc. Natl. Acad. Sci. USA*, **98**, 3197-3202 (2001).

13) Kerppola TK, *Annu Rev Biophys*, **37**, 465-487 (2008).

14) Liu CY, Schroder M, and Kaufman RJ, *J Biol Chem*, **275**, 24881-24885 (2000).

15) Liu CY, Wong HN, Schauerte JA, and Kaufman RJ, *J Biol Chem*, **277**, 18346-18356 (2002).

16) Li H, Korennykh AV, Behrman SL, and Walter P, *Proc. Natl. Acad. Sci. USA*, **107**, 16113-16118 (2010).

17) Zhou J, Liu CY, Back SH, Clark RL, Peisach D, Xu Z, and Kaufman RJ, *Proc. Natl. Acad. Sci. USA*, **103**, 14343-14348 (2006).

18) Trichas G, Begbie J, and Srinivas S, *BMC Biol*, **6**, 40 (2008).

19) Szymczak AL, Workman CJ, Wang Y, Vignali KM, Dilioglou S, Vanin EF, and Vignali DA, *Nat Biotechnol*, **22**, 589-594 (2004).

20) Tirasophon W, Welihinda AA, and Kaufman RJ, *Genes Dev*, **12**, 1812-1824 (1998).

21) Nakagawa T, Zhu H, Morishima N, Li E, Xu J, Yankner BA, and Yuan J, *Nature*, **403**, 98-103 (2000).

22) Gotoh T, Oyadomari S, Mori K, and Mori M, *J Biol Chem*, **277**, 12343-12350 (2002).

23) Muroi M, Kazami S, Noda K, Kondo H, Takayama H, Kawatani M, Usui T, and Osada H, *Chem Biol*, **17**, 460-470 (2010).

24) Aparicio-Fernandez X, Garcia-Gasca T, Yousef GG, Lila MA, Gonzalez de Mejia E, and Loarca-Pina G, *J Agric Food Chem*, **54**, 2116-2122 (2006).

25) Ri M, Tashiro E, Oikawa D, Shinjo S, Tokuda M, Yokouchi Y, Narita T, Masaki A, Ito A, Ding J, Kusumoto S, Ishida T, Komatsu H, Shiotsu Y, Ueda R, Iwawaki T, Imoto M, and Iida S, *Blood Cancer J*, **2**, e79 (2012).

26) Hu CD, and Kerppola TK, *Nat Biotechnol*, **21**, 539-545 (2003).

Figure legends

Fig. 1. DTT induced the reconstitution of cerulean in HeLa/IRE1α-BiFC cells, which stably express IRE1αΔKR-cerN and –cerC.

(A) A schematic illustration of fusion proteins designed for the detection of IRE1α dimerization with the BiFC assay. ss, signal sequence; Lu, luminal domain; T, transmembrane domain; Li, linker domain; K, kinase domain; R, RNase domain; cerN, N-term fragment of cerulean (1-152 a.a.); cerC, C-term fragment of cerulean (155-239 a.a.); 2A, 2A peptide sequence from the insect Thosea asigna virus. The plasmids pCI-neo-IRE1αΔKR-cerN and cerC were constructed as follows: First, a deletion mutant of IRE1α (IRE1αΔKR (1-1662 nucleotides)) was amplified from pcDNA3-IRE1α-FLAG[25] (hereafter, PCR was performed with KOD-plus polymerase (TOYOBO, Osaka, Japan)) and the amplicon was inserted into pCI-neo (Promega, Madison, WI, USA). Cerulean N-term (cerN; 1-462 nucleotides) and C-term (cerC; 463-717 nucleotides) were amplified from pmCerulean-C1 (provided by Dr. Miyawaki). The split site of cerulean was referred to in a previous report[26]. These cerulean fragments were inserted into pCI-neo-IRE1αΔKR at the 3' terminus of IRE1α (pCI-neo-IRE1αΔKR-cerN and cerC). The plasmid designated as pCI-neo-IRE1αΔKR-cerN-2A-IRE1αΔKR-cerC was constructed with PCR using pCI-neo-IRE1αΔKR-cerN as a template, and the amplicon was inserted into pCI-neo-IRE1αΔKR-cerC at the 3' term of cerC.

(B) HeLa or HeLa/IRE1α-BiFC#5 and #10 cells were lysed and the expression of the fusion proteins was detected by western blotting using an anti-FLAG antibody (Sigma Aldrich, St. Louis, MO, USA). The arrows with a solid line and dotted line indicate IRE1αΔKR-cerN and IRE1αΔKR-cerC, respectively. β-actin was immunoblotted as a loading control with anti-β-actin antibody (Sigma Aldrich).

(C) HeLa/IRE1α-BiFC#5 and #10 cells were treated with 3 mM DTT for 1 hour. Then, the cells were fixed and immunostained using anti-FLAG antibody (Sigma Aldrich) and

anti-rabbit IgG tagged with Alexa Fluor 546 (Life Technologies, Carlsbad, CA, USA), and the photos were taken under a confocal microscope (FV1000, Olympus Corp., Tokyo, Japan). Scale bar, 20 μm. All data were representative of at least three independent studies.

Fig. 2. The reconstitution of cerulean and foci formation of IRE1αΔKR-cerN and –cerC were induced by treatment with ER stress inducers.

HeLa/IRE1α-BiFC#5 cells were treated with 30 nM thapsigargin (Santa Cruz Biotechnology), 10 μg/ml tunicamycin, 2 mM 2-deoxyglucose, 10 μg/ml camptothecin or 0.1 μM staurosporine (Sigma Aldrich) for 4 hours. The cells were then fixed and immunostained using anti-FLAG antibody, and observed under a confocal microscope.

Fig. 3. Effects of ER stress inducers on the reconstitution of cerulean and XBP1 mRNA splicing.

HeLa/IRE1α-BiFC#5 cells were treated with 3 mM DTT, 30 nM thapsigargin, 10 μg/ml tunicamycin, or 2 mM 2-deoxyglucose for 1-8 hours. (A) The cells were then fixed and immunostained using anti-FLAG antibody, and observed under a confocal microscope. The ratio of BiFC-positive cells was calculated as described in the manuscript. Values are the means of three independent experiments. Bars, SD. *: $p < 0.05$. (B)(upper panel) Spliced- or unspliced-XBP1 mRNA was detected with RT-PCR. Black arrowheads show the unspliced inactive form of the XBP1 cDNA amplicon (125 bp) and white arrowheads show the spliced active form of the XBP1 cDNA amplicon (99 bp). (lower

panel) The splicing of XBP1 mRNA was quantified using ImageJ software (http://rsb.info.nih.gov/ij/) as follows: band intensity of the active form at each time point was divided by the band intensity of the inactive form at 0 hour. Values are the means of three independent experiments. Bars, SD. *: $p < 0.05$.

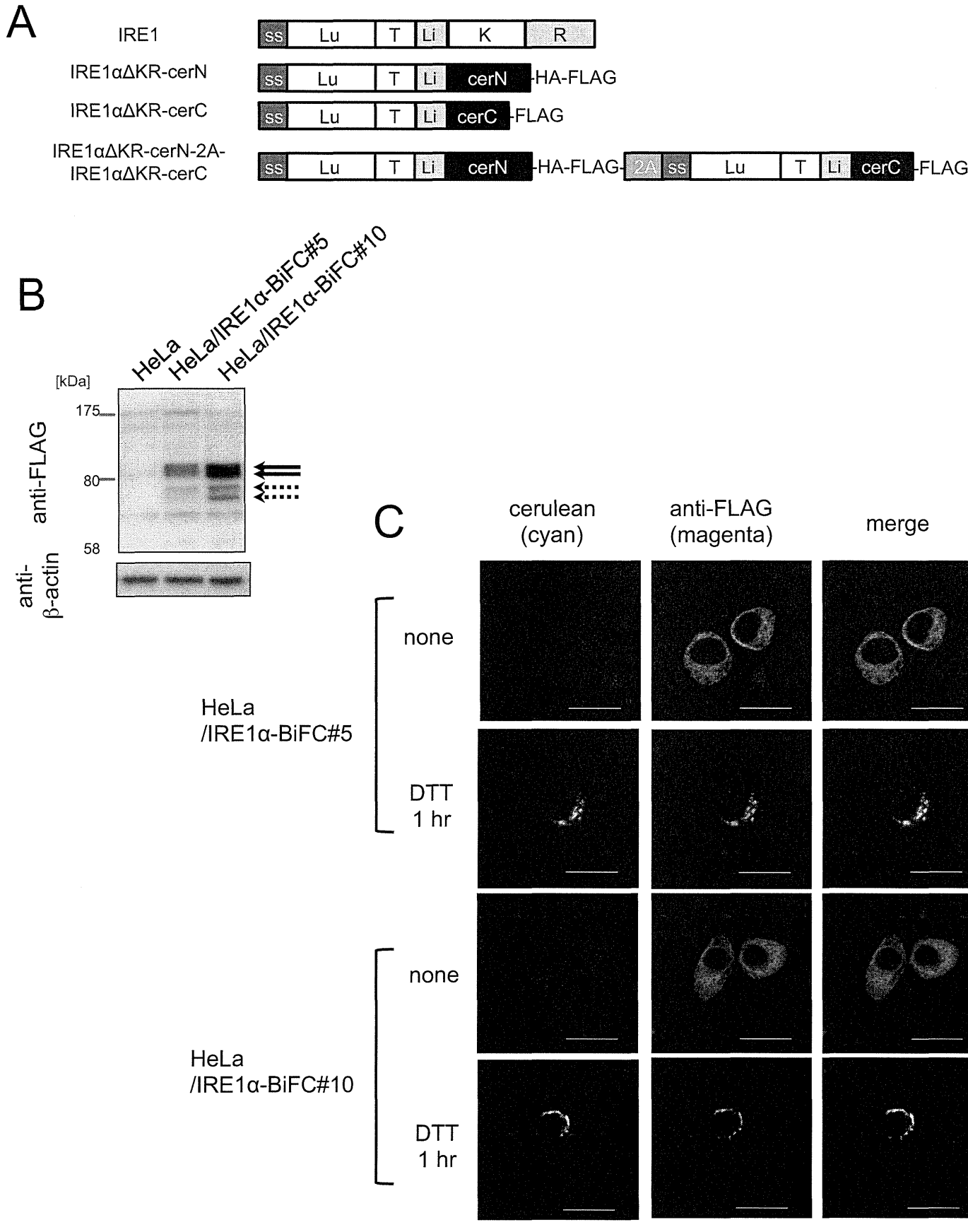
A
IRE1
ss
Lu
T
Li
K
R
IRE1αΔKR-cerN
cerN
HA-FLAG
IRE1αΔKR-cerC
cerC
FLAG
IRE1αΔKR-cerN-2A-
IRE1αΔKR-cerC
2A
B
HeLa
HeLa/IRE1α-BiFC#5
HeLa/IRE1α-BiFC#10
[kDa]
175
80
58
anti-FLAG
anti-
β-actin
C
cerulean
(cyan)
anti-FLAG
(magenta)
merge
none
DTT
1 hr
HeLa
/IRE1α-BiFC#5
HeLa
/IRE1α-BiFC#10

Fig. 1

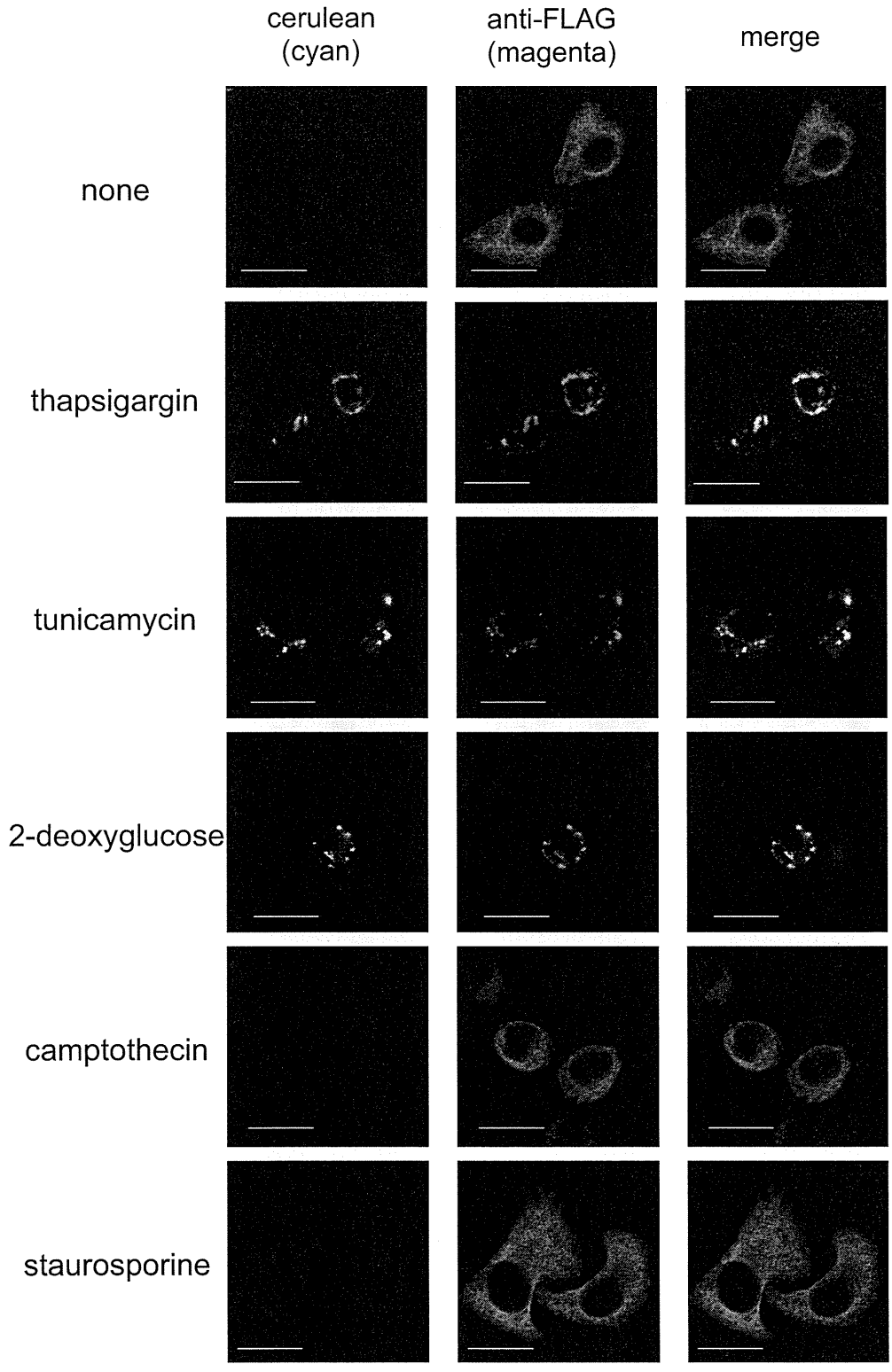
cerulean
(cyan)
anti-FLAG
(magenta)
merge
none
thapsigargin
tunicamycin
2-deoxyglucose
camptothecin
staurosporine

Fig. 2

A

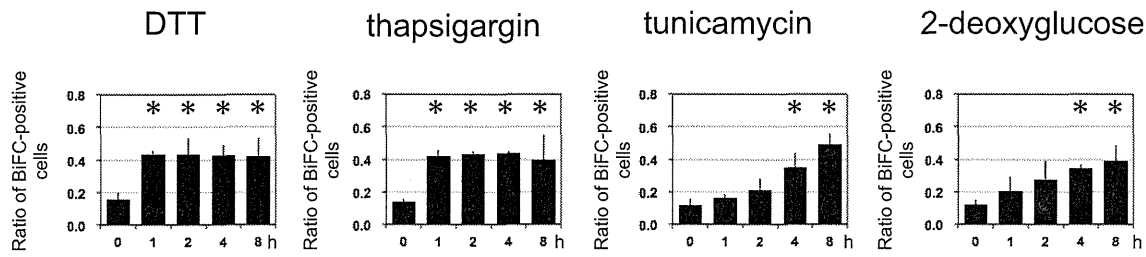
DTT
thapsigargin
tunicamycin
2-deoxyglucose
Ratio of BiFC-positive cells
0.0
0.2
0.4
0.6
0.8
0 1 2 4 8 h
*

B

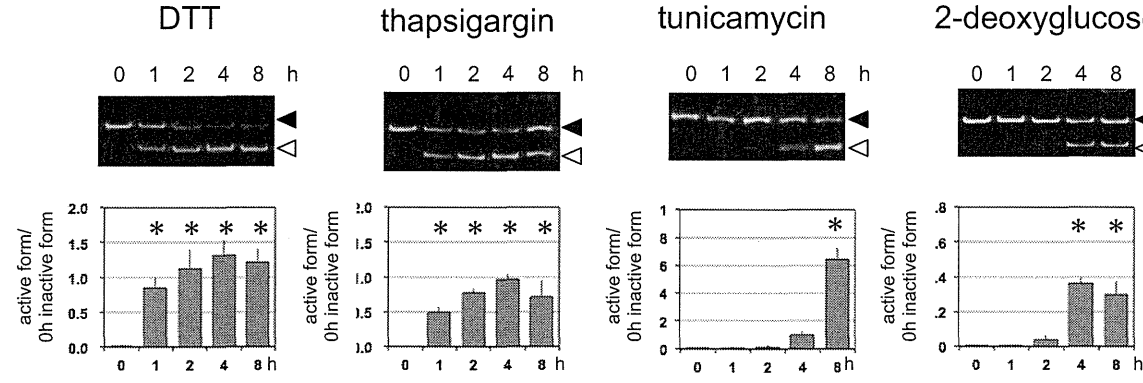
DTT
thapsigargin
tunicamycin
2-deoxyglucose
0 1 2 4 8 h
active form/
0h inactive form
0.0
0.5
1.0
1.5
2.0
*

Fig. 3

Biosci. Biotechnol. Biochem., **77** (4), 729–735, 2013

Comparative Analysis of the Expression Patterns of UPR-Target Genes Caused by UPR-Inducing Compounds

Satoko SHINJO, Yuji MIZOTANI, Etsu TASHIRO,† and Masaya IMOTO

Department of Biosciences and Informatics, Faculty of Science and Technology, Keio University, 3-14-1 Hiyoshi, Kohoku-ku, Yokohama 223-8522, Japan

Received October 19, 2012; Accepted January 10, 2013; Online Publication, April 7, 2013
[doi:10.1271/bbb.120812]

Endoplasmic reticulum (ER) stress, due to an accumulation of unfolded proteins in the ER, leads to a process known as the unfolded protein response (UPR). Since the several compounds used to induce UPR have different modes of action, their mechanisms of protein accumulation are thought to be different, but it is unclear whether these compounds can upregulate UPR target genes with similar kinetics. Hence, we sought to compare the expression patterns of nine UPR target genes induced by seven UPR-inducing compounds. Hierarchical clustering analysis revealed that the expression patterns of the UPR target genes induced by the seven compounds were classified into two clusters; cluster A (thapsigargin, tunicamycin, 2-deoxyglucose, and dithiothreitol) and cluster B (brefeldin A, monensin, and eeyarestatin I). Thus, this study suggests the existence of at least two types of UPR target gene expression profiles, which depend on the mode of action of the compounds.

Key words: unfolded protein response (UPR); endoplasmic reticulum (ER) stress; UPR-inducing compound; profiling

The endoplasmic reticulum (ER) is the organelle in which newly synthesized transmembrane and secreted proteins are folded. Proteins that have undergone the steps of conformational maturation, including folding, glycosylation, and intra/intermolecular disulfide bond formation, can be transported to their destination *via* the Golgi apparatus, but if the proteins have failed to form with the proper conformation, they accumulate in the ER lumen, a condition referred to as ER stress. In order to restore homeostasis in the ER, the cells activate an unfolded protein response (UPR) *via* activation of three ER transmembrane proteins, referred to as ER stress sensors: activating transcription factor 6 (ATF6), inositol-requiring kinase 1 (IRE1), and protein kinase regulated by RNA-like ER kinase (PERK). This is followed by the activation of specific transcription factors: activated ATF6 for ATF6, XBP1 (x-box binding protein 1) for IRE1, and ATF4 (activating transcription factor 4) for PERK. These transcription factors eventually upregulate the expression of UPR target genes to execute four responses: (i) translational attenuation to limit further protein load at the ER; (ii) enhancement of the capacity of the protein folding system through upregulation of ER chaperones or folding enzymes such as glucose-regulated proteins 78 (GRP78, also known as BiP, immunoglobulin-binding protein) and 94 (GRP94), protein disulfide isomerase (PDI), and ER-localized DnaJ 4 (ERdj4); (iii) facilitation of ER-associated degradation (ERAD), which is accelerated by enhancer mannosidase alpha-like 1 (EDEM1); and, (iv) induction of cellular apoptosis, in which C/EBP homologous protein (CHOP) is thought to play an important role if the adaptive responses (i–iii) are insufficient to relieve ER stress (review in refs. 1 and 2).

In most studies, UPR is induced by treating *in vitro* cell models with compounds such as tunicamycin, thapsigargin, and dithiothreitol (DTT), which impair the *N*-linked glycosylation of proteins,[3,4] the Ca^{2+}-dependent chaperone *via* inhibition of ER Ca^{2+} ATPase,[5,6] and protein disulfide bond formation[7,8] respectively. Moreover, brefeldin A, an inhibitor of Golgi-specific brefeldin A resistance factor 1 (GBF1),[9,10] 2-deoxyglucose, an analog of glucose and an inhibitor of *N*-linked glycosylation,[11] and eeyarestatin I, an inhibitor of ERAD,[12] also have been reported to induce UPR.[10,13,14] Since these compounds have different modes of action, the mechanisms of protein accumulation in the ER induced by the various compounds are thought to be different, but it is unclear whether these compounds upregulate all UPR target genes by similar kinetics. Therefore, in order to address our question, we compared the time-course expression profiles of UPR-target genes after treatment with UPR-inducing compounds.

First we first selected six compounds commonly used as UPR inducers: 2-deoxyglucose, brefeldin A, DTT, eeyarestatin I, thapsigargin, and tunicamycin. Exploratory chemical screening indicated that monensin induced the expression of GRP78 and other eight UPR-target genes, so this was added as a prospective UPR inducer (see below). We measured the expression of nine UPR target genes, ATF4, CHOP, EDEM1,

† To whom correspondence should be addressed. Tel: +81-45-566-1793; Fax: +81-45-566-1557; E-mail: tashiro@bio.keio.ac.jp

Abbreviations: ATF4, activating transcription factor 4; ATF6, activating transcription factor 6; CHOP, C/EBP homologous protein; DTT, dithiothreitol; EDEM1, ER degradation enhancer mannosidase alpha-like 1; eIF2α, eukaryotic initiation factor 2 α; ER, endoplasmic reticulum; ERAD, ER-associated degradation; ERdj4, ER-localized DnaJ 4; GADD34, growth arrest- and DNA damage-inducible gene 34; GBF1, Golgi-specific brefeldin A resistance factor 1; GRP78, glucose-regulated protein 78; GRP94, glucose-regulated protein 94; IRE1, inositol-requiring kinase 1; $p58^{IPK}$, protein kinase inhibitor of 58 kDa; PDI, protein disulfide isomerase; PERK, protein kinase regulated by RNA-like ER kinase; RT-PCR, reverse transcription PCR; UPR, unfolded protein response; VSVG, vesicular stomatitis virus G; XBP1, x-box binding protein 1

ERdj4, growth arrest- and DNA damage-inducible gene (GADD) 34, GRP78, GRP94, protein kinase inhibitor of 58 kDa ($p58^{IPK}$), and PDI. GADD34 and $p58^{IPK}$ have been reported to act as feedback regulators of UPR.[15,16] The expression profiles of these genes appeared to show characteristic patterns among the compounds. Hierarchical clustering analysis based on the kinetics of the expression of UPR target genes revealed at least two UPR target gene expression profiles, which were dependent on the mode of action of the UPR-inducing compound.

Materials and Methods

Materials. Tunicamycin, 2-deoxyglucose, monensin, and mouse monoclonal anti-β-actin (AC-74) were purchased from Sigma Aldrich (St. Louis, MO). Brefeldin A and DTT were from Calbiochem (San Diego, CA) and Wako Pure Chemical Industries, (Osaka, Japan) respectively. Thapsigargin and eeyarestatin I were from Santa Cruz Biotechnology (Santa Cruz, CA). Mouse monoclonal anti-KDEL (10C3) was from ENZO Life Sciences (Farmingdale, NY). Rabbit polyclonal anti-eIF2α and anti-phospho eIF2α (Ser51) were from Cell Signaling Technology (Beverly, MA). Rabbit polyclonal anti-PERK was from Rockland (Gilbertsville, PA). Horseradish peroxidase-conjugated anti-mouse IgG secondary antibody was from GE Healthcare (Little Chalfont, UK).

Cell culture. Human epithelial adenocarcinoma cell line HeLa was cultured in Dulbecco's Modified Eagle's Medium (DMEM; Nissui, Tokyo) supplemented with 8% fetal bovine serum at 37 °C in a 5% CO_2–95% air atmosphere.

Western blotting. Western blotting was performed as described previously.[17] Cell pellets were lysed using an extraction buffer containing 150 mM NaCl, 2.5 mM EGTA, 1 mM EDTA, 1 mM DTT, 0.1% Tween-20, 10 mM β-glycerophosphate, 1 mM NaF, 0.1 mM Na_3VO_4, 10% glycerol, and 50 mM HEPES (pH 7.5). Lysates were separated by 7%–10% SDS–PAGE and then subjected to immunoblotting. This was followed by detection using the ECL Western blotting detection system (Millipore, Bedford, MA) and on LAS-1000 CCD camera (Fujifilm, Tokyo). The visualized bands were quantified using ImageJ software (http://rsb.info.nih.gov/ij/).

Real-time RT-PCR. Reverse transcription was carried out as described previously.[18] Total RNA was extracted from HeLa cells and reverse-transcribed. The synthesized cDNA was subjected to quantitative real-time RT-PCR using SYBR premix Ex Taq (Takara, Shiga, Japan), and was detected using Thermal Cycler Dice Real Time System II (Takara). Data were analyzed using the Smart Cycler software program (Multiplate RQ version 1.00; Takara) by the relative quantification method.

Real-time cycle conditions for ERdj4 were 2 min at 50 °C, followed by 10 min at 90 °C, and then 45 cycles, each cycle 95 °C for 30 s and 63 °C for 1 min. The conditions for GAPDH were 10 s at 95 °C and then 35 cycles, each of 95 °C for 3 s, 60 °C for 10 s, and 72 °C for 10 s. RT-PCR conditions for all the other genes were 10 s at 95 °C and then 40 cycles, each cycle 95 °C for 3 s, 60 °C for 10 s, and 72 °C for 15 s. The sequences of the primer sets are shown in Table S1 (see *Biosci. Biotechnol. Biochem.* Web site). The amount of total RNA present in each reaction was normalized using GAPDH as internal control. Data are averages of at least three separate experiments, and one outlier was omitted in each case by Dixon's Q-test at the 99% confidence level.[19]

RNA interference. siRNA double-stranded oligonucleotides designed to interfere with the expression of PERK (HSS190343; Life Technologies) with siRNA as negative control (12935-300; Life Technologies) were used. Transfection of siRNA was demonstrated using Lipofectamine 2000 (Life Technologies) following the manufacturer's instructions. Briefly, HeLa cells were transfected with OPTI-MEM (Life Technologies) including siRNA and Lipofectamine 2000. Twenty-four h after transfection, the cells were trypsinized and seeded into 6-well plates. After further 24 h, the cells were treated with monensin and subjected to Western blotting.

Data processing and hierarchical clustering. The data acquired were normalized among genes and named "UPR fingerprints of genes," or reordered by compound and named "UPR fingerprints of compounds." Pearson's correlation coefficients between the UPR fingerprints were calculated, and these were used to determine degrees of similarity. Hierarchical clustering by an average linkage method was done using R version 2.13.1. (http://www.R-project.org).

Trypan blue dye exclusion assay. Cell viability was evaluated by trypan blue dye exclusion assay, as described previously.[20]

Results

Effects of the six UPR-inducing compounds on cell viability and GRP78 and GRP94 protein expression

Our first investigation was to determine suitable concentrations of six compounds (2-deoxyglucose, brefeldin A, DTT, eeyarestatin I, thapsigargin, and tunicamycin) for induction of UPR. GRP78 and GRP94 are well-known UPR marker proteins. Since the anti-KDEL antibody recognizes the KDEL sequence, a very common ER retention signal, it mainly detected both GRP78 and GRP94. Hence, using the anti-KDEL antibody, protein expression of them was examined in HeLa cells after 24-h of treatment with each of the six compounds (Fig. 1). As shown in Fig. 1A, 2-deoxyglucose induced the expression of GRP78 in a dose-dependent manner, with an approximately 1.5-fold increase at 0.2 mM and a maximum increase at 2 mM, and neither dose affected cell viability. Similarly, brefeldin A, thapsigargin, and tunicamycin also increased the expression of GRP78 in a dose-dependent manner, with maximum increases at 50 ng/mL, 30 nM, and 10 μg/mL, and with moderate increases (approximately 1.5-fold) at 15 ng/mL, 1 nM, and 1 μg/mL respectively. These doses also failed to affect cell viability (Fig. 1B, E, and F). DTT and eeyarestatin I induced GRP78 expression, at 3 mM and 3 μm respectively (Fig. 1C and D). Additionally, each of the compounds, except for brefeldin A, induced the expression of GRP94 similarly to GRP78, but the intensities of GRP78 and GRP94 protein expression induced by the various compounds were different. Upon treatment by brefeldin A, the expression of GRP94 increased in a dose-dependent manner. It reached a maximum at 50 ng/mL and then declined. Thus, it is likely that the expression patterns and the intensities of GRP78 and GRP94 induction were different among the compounds. In this study, the concentrations sufficient to induce maximum and moderate levels of UPR were defined with reference to the expression of GRP78 as to protein level, as summarized in Table 1.

Measurement of the time-course expression of the mRNA levels of nine UPR-target genes

To compare the expression patterns of UPR-target genes induced by the six UPR-inducing compounds, first we measured the mRNA levels of GPR78. HeLa cells were treated with one of the six compounds at the concentrations indicated in Table 1 and the amount of GRP78 mRNA was measured by real-time reverse transcription PCR (RT-PCR). As shown in Fig. 2, all six compounds increased the amount of GRP78 mRNA.

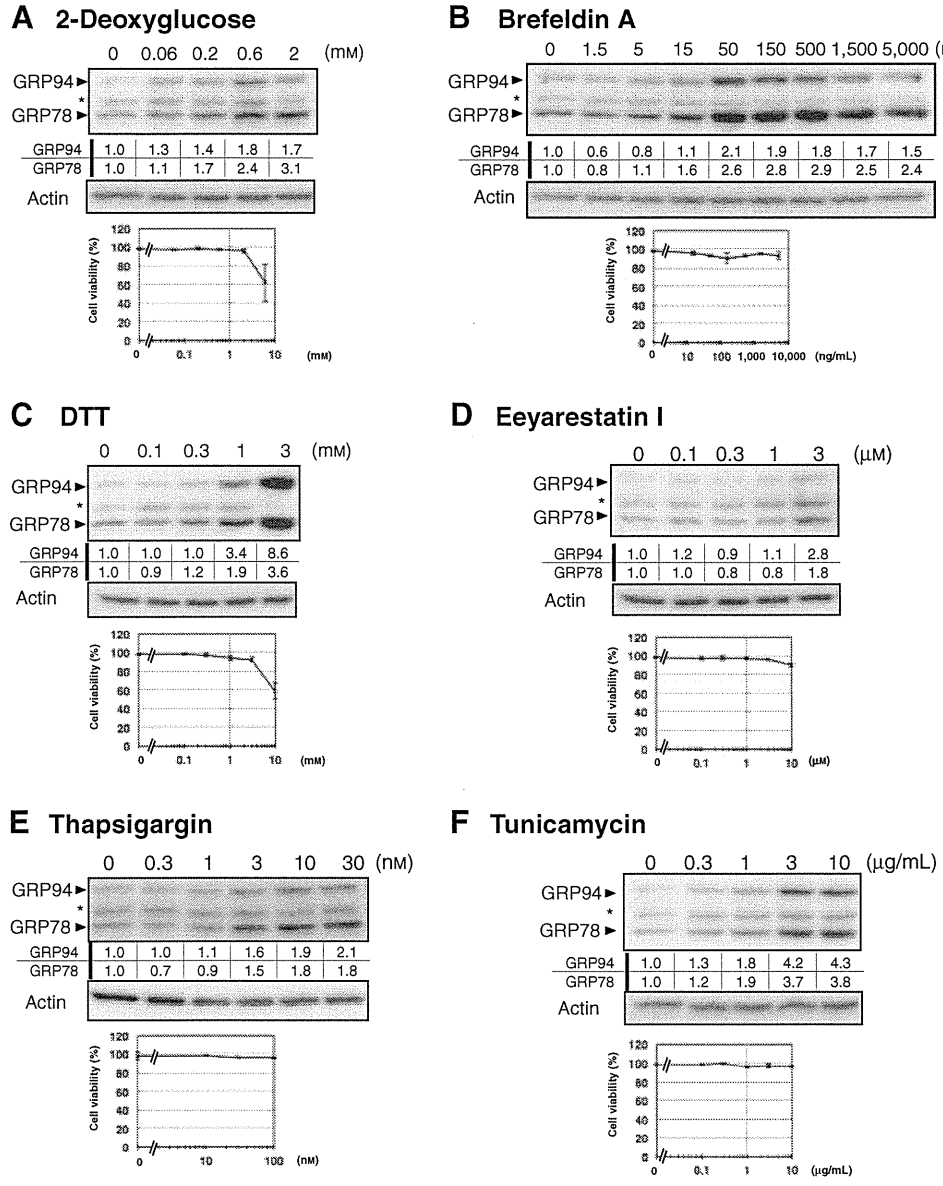

Fig. 1. UPR-Inducing Compounds Induced GRP78 Expression without Affecting Cell Viability.
Biological activity of six UPR-inducing compounds: 2-deoxyglucose (A), brefeldin A (B), DTT (C), eeyarestatin I (D), thapsigargin (E), and tunicamycin (F) (upper panel) HeLa cells were treated with the indicated concentrations of the compounds for 24 h. GRP78 and GRP94 were detected by immunoblotting with the anti-KDEL antibody. *Nonspecific band. The intensities of the bands of GRP78 and GRP94 were divided by that of β-actin and are indicated below the bands (lower panel) HeLa cells were treated with the indicated concentrations of the compounds for 24 h. Cell viability was assessed by trypan blue dye exclusion assay. Values are means of three independent determinations. Bars, SD.

Table 1. Concentrations of UPR-Inducing Compounds

Compound	Concentration	
	Inducing maximum GRP78 levels	Inducing moderate GRP78 levels
Thapsigargin	30 nM	1 nM
Tunicamycin	10 μg/mL	1 μg/mL
2-Deoxyglucose	2 mM	0.2 mM
DTT	3 mM	—
Brefeldin A	50 ng/mL, 5,000 ng/mL	15 ng/mL
Eeyarestatin I	3 μM	—

For instance, 30 nM thapsigargin increased it after 4-h of treatment, and it reached a plateau at an approximately 10-fold increase after 12-h of treatment. Two mM 2-deoxyglucose and 10 μg/mL tunicamycin also increased the amount of GRP78 mRNA, which peaked after approximately 12–16 h of treatment, resulting in 20- and 15-fold increases respectively, and then declined by the end of the 24-h treatment period (Fig. 2). When the cells were treated with 50 ng/mL of brefeldin A, the amount of GRP78 mRNA increased in a time-dependent manner for 24 h, showing an approximately 8-fold rise in expression (Fig. 2). Taken together, the time-course expression data for GRP78 mRNA appeared to show characteristic patterns among the six compounds.

Moreover, there were similar expression patterns for GRP78 mRNA when the HeLa cells were treated with 15 ng/mL, 50 ng/mL, or 5,000 ng/mL of brefeldin A. Furthermore, when the cells were treated with 0.2 mM and 2 mM of 2-deoxyglucose or 1 nM and 30 nM of thapsigargin, the expression patterns of GRP78 mRNA were also similar. In addition, 1 μg/mL of tunicamycin showed a slightly delayed expression pattern for GRP78 mRNA as compared to 10 μg/mL tunicamycin. Overall,

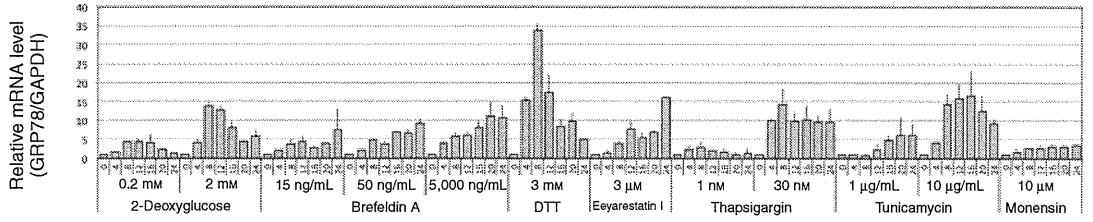

Fig. 2. UPR-Inducing Compounds Increased the Amount of GRP78 mRNA in the HeLa Cells.
HeLa cells were treated with UPR-inducing compounds at the indicated concentrations for 4–24 h. The relative mRNA levels of GRP78 were quantified by real-time RT-PCR. All values were normalized using GAPDH as internal control. Values are means of three independent determinations. Bars, SD.

the differences in the concentrations of the compounds did not have any notable effect on the expression patterns of GRP78 mRNA.

We further measured the changes in the amount of mRNA of an additional eight UPR target genes, ATF4, CHOP, EDEM1, ERdj4, GADD34, GRP94, PDI, and p58^{IPK}, when the cells were treated with each of the six compounds. As shown in Supplemental Fig. 1, all the compounds increased the amounts of the eight UPR target gene mRNA, at the concentrations indicated in Table 1.

Monensin upregulated UPR target genes

An in-house chemical library, which included commercially available compounds as well as compounds of microbial origin in our laboratory, was screened for additional potential UPR-inducing compounds. It was found that monensin, a compound first isolated from *Streptomyces cinnamonensis* and known as a Na^+ ionophore,[21] increased the amount of GRP78 at protein level with 10 μM treatment (Fig. 3A) without affecting cell viability (Fig. 3B). Monensin also increased the amount of GRP78 mRNA slightly at 4–24 h of treatment (Fig. 2), as well as the other eight UPR target genes of interest (Fig. S1). Furthermore, it induced phosphorylation of eIF2α, a well-known substrate of PERK[22] (Fig. 3C). Since four kinases (PERK, PKR, HRI, and GCN2) are known to phosphorylate eIF2α, we examined to determine whether monensin-induced phosphorylation of eIF2α occurs through PERK activation. As shown in Fig. 3C, monensin-induced phosphorylation of eIF2α was impaired in siPERK-transfected HeLa cells, in which successful knockdown of PERK was confirmed by immunoblotting (Fig. 3C), suggesting that monensin activated PERK. Thus, it appears that monensin induced UPR, and hence it was used in the remaining experiments in our study.

Clustering of compounds based on the expression profiles of the UPR target genes

It was observed that the kinetics of UPR target gene expression showed characteristic patterns among the 12 experimental conditions tested (seven compounds, some with multiple concentrations). The data acquired were analyzed by hierarchical clustering with the aim of classifying the expression profiles of the UPR target genes. The real-time RT-PCR data for each UPR target gene obtained under the 12 experimental conditions were normalized to acquire UPR fingerprints of genes. Furthermore, the normalized data were reordered by condition in order to acquire UPR fingerprints of

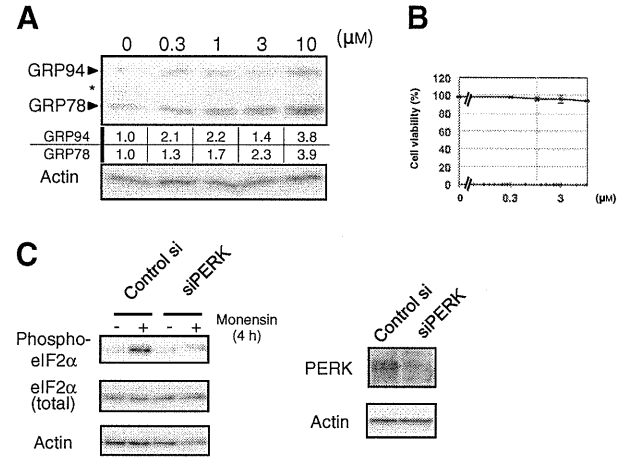

Fig. 3. Monensin Induced UPR.
The biological activity of monensin. (A) HeLa cells were treated with the indicated concentrations of monensin for 24 h. GRP78 and GRP94 were detected by immunoblotting with anti-KDEL antibodies. *Nonspecific band. The band intensities of GRP78 and GRP94 were divided by that of β-actin, and are indicated below the bands. (B) HeLa cells were treated with the indicated concentrations of monensin for 24 h. Cell viability was assessed by trypan blue dye exclusion assay. Values are means of three independent determinations. Bars, SD. (C) Control or PERK siRNA-transfected HeLa cells were treated with 10 μM monensin for 4 h. Total eIF2α and phospho-eIF2α were detected by immunoblotting. Successful knockdown of PERK by siRNA was confirmed by immunoblotting with anti-PERK antibody. β-Actin was immunoblotted as loading control.

compounds (Fig. 4). Each type of fingerprint was analyzed by hierarchical clustering using Pearson's correlation coefficient as a similarity and average-linkage method. As a result of clustering analysis of the compounds, as shown on the left side of Fig. 5, the 12 conditions were divided into two groups: cluster A and cluster B. Cluster A contained thapsigargin, tunicamycin, 2-deoxyglucose, and DTT, and cluster B contained brefeldin A, monensin, and eeyarestatin I. When thapsigargin, tunicamycin, 2-deoxyglucose, or brefeldin A was used at different concentrations, the expression patterns of the UPR target genes were still to be classified in the same cluster. Furthermore, as a result of clustering analysis of the genes, as shown at the top of Fig. 5, nine genes were classifiable into two groups: cluster I and cluster II (Fig. 5). Cluster I contained GRP78, ERdj4, EDEM1, p58^{IPK}, and GRP94, and cluster II contained GADD34, CHOP, PDI, and ATF4. Based on two-way clustering analysis, a heat map displayed the expression data for each gene under each condition by reordering of the data by rows and columns

(Fig. 5), indicated that the expression intensity of cluster I genes in the fingerprints of cluster A was higher than in cluster B; conversely, the expression intensity of cluster II genes in the fingerprints of cluster A was lower than in cluster B.

Discussion

In this study, by hierarchical clustering analysis, the expression patterns of UPR target genes induced by seven compounds were classified into two clusters.

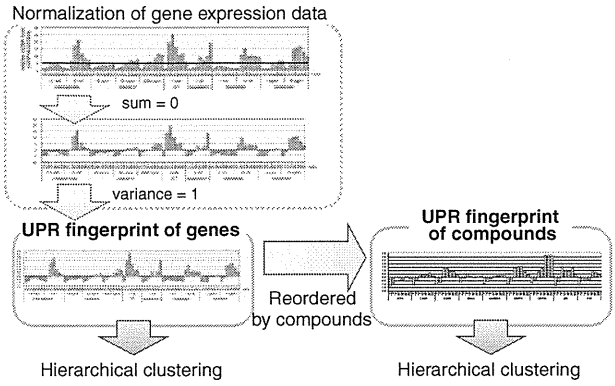

Fig. 4. Schematic Illustration of Method of Data Analysis.
The relative mRNA levels of the genes were normalized by subtracting the average value from the result at each time point and dividing by the standard derivative. A UPR fingerprint of genes was obtained. We created a separate UPR fingerprint of compounds by reordering the data compound-by-compound. Similarities between the two UPR fingerprints (Pearson's correlation coefficient) were calculated and analyzed by hierarchical clustering.

When cells were treated with thapsigargin, tunicamycin, 2-deoxyglucose, or brefeldin A at different concentrations, the expression patterns of the UPR-target genes were grouped into the same cluster (Fig. 5). This suggests that this grouping is due to the difference in the modes of action of the compounds, rather than their concentrations. The compounds comprising cluster A, thapsigargin, tunicamycin, 2-deoxyglucose, and DTT, showed a distinct mode of action, but they have been reported to inhibit the conformational maturation of proteins in the ER,[4,23–26] as described above in the introduction, leading to an accumulation of incorrectly folded proteins in the ER. On the other hand, among the compounds in cluster B, brefeldin A has been reported to accumulate correctly folded conformation of the vesicular stomatitis virus G (VSVG) protein, as judged by detection by the I14 antibody, which recognizes only the native or correctly folded conformation of the VSVG protein.[27,28] Thus, it is likely that the compounds in cluster B induced the expression of UPR target genes by accumulation of excess amounts of correctly folded proteins rather than incorrectly folded proteins in the ER. If this is the case, the difference in the expression patterns of UPR target genes as between cluster A and cluster B are related to the folding status of the accumulated proteins in the ER caused by the compounds in cluster A and cluster B. Eeyarestatin I and monensin were classified into cluster B, with the expectation that eeyarestatin I and monensin can accumulate excess amounts of correctly folded proteins in the ER. Indeed, eeyarestatin I has been reported to accumulate properly folded proteins as a consequence of

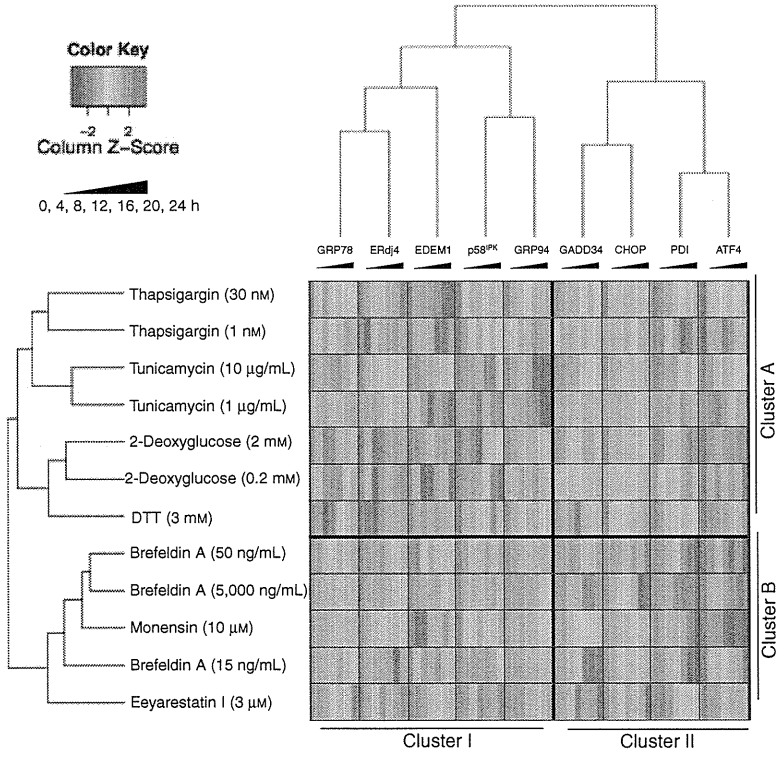

Fig. 5. Two-Dimensional Clustering Analysis of Genes and UPR-Inducing Compounds on the Basis of Pearson's Correlation Coefficients.
UPR fingerprints were analyzed by hierarchical cluster analysis. Dataset of 12 conditions and of nine genes were clustered by the average-linkage method using Pearson's correlation coefficients. Rows indicate seven different small molecular compounds (some with multiple concentrations; therefore 12 conditions). Columns indicate the nine UPR target genes, including the seven different time points. The heat map shows a gradient color scale from green, indicating the score in UPR fingerprint of compounds negative, to red, indicating the score positive, interpolated over gray for the score zero. The seven compounds and the nine genes were clustered into two groups, respectively.

ERAD inhibition, detecting properly folded MHC class I by W6/32 antibody,[12,29] but we cannot exclude the possibility that eeyarestatin I induces UPR through an accumulation of incorrectly folded proteins. On the other hand, monensin has been reported to neutralize acidic intracellular compartments such as the *trans*-Golgi apparatus *via* its ionophore activity, and to inhibit *medial*- to *trans*-Golgi protein transport.[30–32] Hence, we cannot exclude the possibility that inhibition of *medial*- to *trans*-Golgi protein transport by monensin abrogates the entire protein transport system, including transport from the ER to the Golgi apparatus, resulting in an accumulation of correctly folded proteins in the ER. This possibility was confirmed by our observation that another polyether K^+/H^+ ionophore, nigericin, which disrupts Golgi function similarly to monensin,[30,33] also upregulated GRP78 protein expression (Fig. S2).

What remains unclear is the reason the compounds in cluster A and cluster B induced different expression patterns of the UPR target genes (Fig. 5). As shown in Fig. 5, the compounds in cluster A and cluster B comparatively highly upregulated the genes belonging to cluster I, GRP78, ERdj4, EDEM1, $p58^{IPK}$, and GRP94, and cluster II, GADD34, CHOP, PDI, and ATF4, respectively. Since the expression of a UPR target gene is transcriptionally regulated by the activation of three ER stress sensors (ATF6, IRE1, and PERK), it is possible that each of these stress sensors has distinct sensitivity to compounds belonging to cluster A and cluster B, resulting in higher expression of the genes in cluster I and cluster II respectively. Indeed, it has been reported that GRP94 and GRP78 are regulated by ATF6,[34,35] ERdj4 is regulated by IRE1,[36–38] and EDEM1 and $p58^{IPK}$ are regulated by both IRE1 and ATF6.[34,37,38] On the other hand, among the genes to be classified in cluster II, the expression of GADD34 and CHOP was reported to be regulated by PERK.[15,39,40] Furthermore, since a previous study found that the PDI gene has a sequence resembling the ATF-binding site in its promoter region,[41] the expression of PDI, a gene in cluster II, might also be mediated by ATF4 and its upstream ER stress sensor, PERK. Thus, it is likely that ATF6 and IRE1 are sensitive to compounds in cluster A in comparison with PERK, and that PERK is sensitive to compounds in cluster B as compared to ATF6 and IRE1. On the other hand, among the compounds in the same cluster, little difference in the expression patterns of the UPR target genes was observed. For instance, tunicamycin highly upregulated $p58^{IPK}$ and GRP94 as compared to thapsigargin, 2-deoxyglucose, and DTT. 2-Deoxyglucose and DTT highly upregulated GRP78 and ERdj4 as compared to thapsigargin and tunicamycin. In order to compare these differences more clearly, we are developing a new detection system to monitor the activation kinetics of the three ER stress sensors.

In summary, we classified the expression patterns of nine UPR target genes induced by seven UPR-inducing compounds into two clusters by hierarchal clustering analysis. Our results suggest the existence of at least two types of UPR target gene expression profiles, which might be dependent on the mode of action of the compounds. To our knowledge, although there have been many reports on the regulatory mechanism of UPR target gene expression using UPR-inducing compounds, they have failed to address the question whether the difference in mode of action of the UPR-inducing compounds influences the expression patterns of UPR target genes. This study is a first approach this question by statistical analysis, and provides the information that the expression patterns of UPR target genes are indeed different among the compounds. We hypothesize that the sensitivity of the three ER stress sensors depends on the folding status of the accumulated proteins in the ER, which results in the different expression patterns of the UPR target genes. Further study is needed to elucidate our hypothesis that the folding status of the accumulated proteins affects the activation of ER stress sensors, the expression of UPR target genes, and consequent responses, such as protein refolding, protein degradation, and apoptosis.

Acknowledgments

This work is supported by Grants-in-Aid for Scientific Research (KAKENHI grant no. 23510283, to E.T.) from Ministry of Education, Culture, Sports, Science and Technology (MEXT), Japan. S.S. was a research assistant in the Global COE Program for Human Metabolomic Systems Biology.

References

1) Ron D and Walter P, *Nat. Rev. Mol. Cell Biol.*, **8**, 519–529 (2007).
2) Zhao L and Ackerman SL, *Curr. Opin. Cell Biol.*, **18**, 444–452 (2006).
3) Olden K, Pratt RM, Jaworski C, and Yamada KM, *Proc. Natl. Acad. Sci. USA*, **76**, 791–795 (1979).
4) Takatsuki A, Kohno K, and Tamura G, *Agric. Biol. Chem.*, **39**, 2089–2091 (1975).
5) Price BD, Mannheim-Rodman LA, and Calderwood SK, *J. Cell. Physiol.*, **152**, 545–552 (1992).
6) Thastrup O, Cullen PJ, Drøbak BK, Hanley MR, and Dawson AP, *Proc. Natl. Acad. Sci. USA*, **87**, 2466–2470 (1990).
7) Cleland WW, *Biochemistry*, **3**, 480–482 (1964).
8) Halleck MM, Holbrook NJ, Skinner J, Liu H, and Stevens JL, *Cell Stress Chaperones*, **2**, 31–40 (1997).
9) Citterio C, Vichi A, Pacheco-Rodriguez G, Aponte AM, Moss J, and Vaughan M, *Proc. Natl. Acad. Sci. USA*, **105**, 2877–2882 (2008).
10) Liu E and Ou J, *J. Biol. Chem.*, **267**, 7128–7133 (1992).
11) Datema R and Schwarz RT, *Biochem. J.*, **184**, 113–123 (1979).
12) Fiebiger E, Hirsch C, Vyas JM, Gordon E, Ploegh HL, and Tortorella D, *Mol. Biol. Cell*, **15**, 1635–1646 (2004).
13) Wang Q, Mora-Jensen H, Weniger MA, Perez-Galan P, Wolford C, Hai T, Ron D, Chen W, Trenkle W, Wiestner A, and Ye Y, *Proc. Natl. Acad. Sci. USA*, **106**, 2200–2205 (2009).
14) Watowich SS and Morimoto RI, *Mol. Cell. Biol.*, **8**, 393–405 (1988).
15) Novoa I, Zeng H, Harding HP, and Ron D, *J. Cell Biol.*, **153**, 1011–1022 (2001).
16) Yan W, Frank CL, Korth MJ, Sopher BL, Novoa I, Ron D, and Katze MG, *Proc. Natl. Acad. Sci. USA*, **99**, 15920–15925 (2002).
17) Sasazawa Y, Futamura Y, Tashiro E, and Imoto M, *Cancer Sci.*, **100**, 1460–1467 (2009).
18) Tashiro E, Hironiwa N, Kitagawa M, Futamura Y, Suzuki S, Nishio M, and Imoto M, *J. Antibiot.*, **60**, 547–553 (2007).
19) Dean R and Dixon W, *Anal. Chem.*, **23**, 636–638 (1951).
20) Kawamura T, Matsubara K, Otaka H, Tashiro E, Shindo K, Yanagita RC, Irie K, and Imoto M, *Bioorg. Med. Chem.*, **19**, 4377–4385 (2011).
21) Haney ME Jr and Hoehn MM, *Antimicrob. Agents Chemother.*, **7**, 349–352 (1967).

22) Harding HP, Zhang Y, and Ron D, *Nature*, **397**, 271–274 (1999).
23) Di Jeso B, Ulianich L, Pacifico F, Leonardi A, Vito P, Consiglio E, Formisano S, and Arvan P, *Biochem. J.*, **370**, 449–458 (2003).
24) Kurtoglu M, Gao N, Shang J, Maher JC, Lehrman MA, Wangpaichitr M, Savaraj N, Lane AN, and Lampidis TJ, *Mol. Cancer Ther.*, **6**, 3049–3058 (2007).
25) Schwarz RT, Schmidt MF, and Datema R, *Biochem. Soc. Trans.*, **7**, 322–326 (1979).
26) Kaufman RJ, *Genes Dev.*, **13**, 1211–1233 (1999).
27) Lefrancois L and Lyles DS, *Virology*, **121**, 157–167 (1982).
28) Preston AM, Gurisik E, Bartley C, Laybutt DR, and Biden TJ, *Diabetologia*, **52**, 2369–2373 (2009).
29) Parham P, Barnstable CJ, and Bodmer WF, *J. Immunol.*, **123**, 342–349 (1979).
30) Dinter A and Berger EG, *Histochem. Cell Biol.*, **109**, 571–590 (1998).
31) Griffiths G, Quinn P, and Warren G, *J. Cell Biol.*, **96**, 835–850 (1983).
32) Mollenhauer HH, Morre DJ, and Rowe LD, *Biochim. Biophys. Acta*, **1031**, 225–246 (1990).
33) Craig S and Goodchild DJ, *Protoplasma*, **122**, 91–97 (1984).
34) Yamamoto K, Sato T, Matsui T, Sato M, Okada T, Yoshida H, Harada A, and Mori K, *Dev. Cell*, **13**, 365–376 (2007).
35) Yoshida H, Haze K, Yanagi H, Yura T, and Mori K, *J. Biol. Chem.*, **273**, 33741–33749 (1998).
36) Kanemoto S, Kondo S, Ogata M, Murakami T, Urano F, and Imaizumi K, *Biochem. Biophys. Res. Commun.*, **331**, 1146–1153 (2005).
37) Lee AH, Iwakoshi NN, and Glimcher LH, *Mol. Cell. Biol.*, **23**, 7448–7459 (2003).
38) Yoshida H, Matsui T, Hosokawa N, Kaufman RJ, Nagata K, and Mori K, *Dev. Cell*, **4**, 265–271 (2003).
39) Harding HP, Novoa I, Zhang Y, Zeng H, Wek R, Schapira M, and Ron D, *Mol. Cell*, **6**, 1099–1108 (2000).
40) Ma Y and Hendershot LM, *J. Biol. Chem.*, **278**, 34864–34873 (2003).
41) Tasanen K, Oikarinen J, Kivirikko KI, and Pihlajaniemi T, *J. Biol. Chem.*, **267**, 11513–11519 (1992).

The Journal of Antibiotics (2013) 66, 165–170

www.nature.com/ja

ORIGINAL ARTICLE

Novel derivatives of aclacinomycin A block cancer cell migration through inhibition of farnesyl transferase

Shigeyuki Magi[1,3], Tetsuo Shitara[2,3], Yasushi Takemoto[1], Masato Sawada[1], Mitsuhiro Kitagawa[1], Etsu Tashiro[1], Yoshikazu Takahashi[2] and Masaya Imoto[1]

In the course of screening for an inhibitor of farnesyl transferase (FTase), we identified two compounds, *N*-benzyl-aclacinomycin A (ACM) and *N*-allyl-ACM, which are new derivatives of ACM. *N*-benzyl-ACM and *N*-allyl-ACM inhibited FTase activity with IC_{50} values of 0.86 and 2.93 μM, respectively. Not only ACM but also C-10 epimers of each ACM derivative failed to inhibit FTase. The inhibition of FTase by *N*-benzyl-ACM and *N*-allyl-ACM seems to be specific, because these two compounds did not inhibit geranylgeranyltransferase or geranylgeranyl pyrophosphate (GGPP) synthase up to 100 μM. In cultured A431 cells, *N*-benzyl-ACM and *N*-allyl-ACM also blocked both the membrane localization of H-Ras and activation of the H-Ras-dependent PI3K/Akt pathway. In addition, they inhibited epidermal growth factor (EGF)-induced migration of A431 cells. Thus, *N*-benzyl-ACM and *N*-allyl-ACM inhibited EGF-induced migration of A431 cells by inhibiting the farnesylation of H-Ras and subsequent H-Ras-dependent activation of the PI3K/Akt pathway.
The Journal of Antibiotics (2013) **66,** 165–170; doi:10.1038/ja.2012.108; published online 30 January 2013

Keywords: aclacinomycin A; cancer cell migration; farnesyl transferase

INTRODUCTION

Cell migration is not only a central feature of a range of physiological processes, but also a crucial event in the spread of cancer and, consequently, the metastatic process.[1] Ras protein, a guanine nucleotide (GTP) binding protein, has an important role in signal transduction and regulation of cell migration.[2,3] A series of post-translational modifications are essential for the cell membrane association of Ras protein. One key modification is farnesylation of Ras by farnesyl transferase (FTase) on the C-terminus cystein residue of the CAAX motif.[4] Previously, we screened for inhibitors of cancer cell migration and obtained moverastin A and B, new members of the cylindrol family, from *Aspergillus* sp. F7720.[5] Furthermore, we found that moverastin A and B inhibited FTase, and demonstrated that moverastins inhibited the migration of tumor cells by inhibiting the farnesylation of H-Ras. However, the inhibitory activity of moverastins for FTase was rather modest (IC_{50} value of 14.7 μM). Thus we started screening of potent inhibitors of FTase as part of the project in Screening Committee of Anticancer Drugs (SCADS). In this study, we found new inhibitors of FTase, *N*-benzyl-aclacinomycin A (ACM) and *N*-allyl-ACM, which are chemically synthesized derivatives of ACM (aclarubicin) and described the antimigrative effect of these compounds.

MATERIALS AND METHODS

General experimental procedures

Centrifugal partition chromatography was performed using a centrifugal partition chromatograph-L.L.N. (Model-NMF, 250 ml cell; Sanki Engineering, Tokyo, Japan). HRMS were recorded on an Accu TOF-T100LC (JEOL, Tokyo, Japan) mass spectrometer. ^{1}H-NMR and ^{13}C-NMR data were measured on a JEOL ECX-600 spectrometer. Chemical shifts for proton are reported in p.p.m. downfield from tetramethylsilane. For ^{13}C NMR, chemical shifts were reported in the scale relative to NMR solvent ($CDCl_3$: 77.0 p.p.m.) as an internal reference. Optical rotations were measured with a P-1030 polarimeter (JASCO, Tokyo, Japan). IR spectra were recorded on a FT/IR-4100 Fourier transform IR spectrometer (JASCO).

Preparation of *N*-benzyl-ACM

ACM hydrochloride (255.9 mg, 0.301 mM) in dry dimethylformamide (5.2 ml) was treated with benzyl bromide (0.108 ml, 3.0 equiv.) in the presence of diisopropylethylamine (0.315 ml, 6.0 equiv.) at room temperature for 19 h. After removal of the solvent, the residue was dissolved in $CHCl_3$, washed with H_2O and then continuously with aqueous Na_2SO_4. The $CHCl_3$ layer was dried over Na_2SO_4 and evaporated. The oily residue was washed with hexane-diethyl ether (4:1) three times and the remaining residue (crude material **1**) (328.4 mg) was purified by centrifugal partition chromatography ($CHCl_3$: CH_3OH: H_2O = 5:6:4, ascending mode), to give mixtures containing

[1]Faculty of Science and Technology, Department of Biosciences and Informatics, Keio University, Yokohama, Japan and [2]Institute of Microbial Chemistry (BIKAKEN), Tokyo, Japan
Correspondence: Professor M Imoto, Faculty of Science and Technology, Department of Biosciences and Informatics, Keio University, Yokohama 223-8522, Japan.
E-mail: imoto@bio.keio.ac.jp
or Professor Y Takahashi, Institute of Microbial Chemistry (BIKAKEN), 3-14-23 Kamiosaki, Shinagawa-ku, Tokyo 141-0021, Japan.
E-mail: Takahashiy@bikaken.or.jp
[3]These authors contributed equally to this work.
Received 25 September 2012; revised 1 November 2012; accepted 9 November 2012; published online 30 January 2013

N-benzyl-ACM (151.28 mg). The portion (118.6 mg) of obtained crude materials was passed through a Dowex 1 × 2 (chloride form, CH_3OH: H_2O = 1:4), and finally purified by silica gel column chromatography ($CHCl_3$: CH_3OH: H_2O = 10:1:0.1), to give pure *N*-benzyl-ACM (71.4 mg, yield 32%) as an orange powder.

HRMS (ESI$^+$ mode): *m/z* 902.39627 (observed), *m/z* 902.39575 (calcd. for $C_{49}H_{60}NO_{15}^+$); ^{1}H-NMR of rhodosamine and D-ring moieties (chemical shift in p.p.m., splitting pattern, *J* in Hz) in $CDCl_3$: H-7 (5.18, d, 5.5), H-8a (2.20, d, 15.0), H-8b (2.61, dd, 5.5 and 15.0), 9-OH (4.57, br s), H-10 (4.12, s), H-13a (1.69, dq, 7.5 and 15.0), H-13b (1.79, dq, 7.5 and 15.0), H-14 (1.15, t, 7.5), -COOMe (3.69, s), H-1′ (5.81, br d, 2.0), H-2′a (overlapping at around 2.1 p.p.m.), H-2′b (overlapping at around 2.4 p.p.m.), H-3′ (5.13, br d, 14.0), H-4′ (4.45, br s), H-5′ (overlapping at around 4.55p.p.m.), H-6′ (1.38, d, 7.0). *Optical rotation*: $[\alpha]_D^{26}$ +23 (*c* 0.1, $CHCl_3$) NMR table of *N*-benzyl-ACM is presented in Table 1.

Preparation of *N*-allyl-ACM

ACM hydrochloride (259.2 mg, 0.305 mM) in dry dimethylformamide (5.2 ml) was treated with allyl iodide (0.042 ml, 1.5 equiv.) in the presence of diisopropylethylamine (0.16 ml, 3.0 equiv.) at room temperature for 24 h. The reagents allyl iodide (0.028 ml, 1.0 equiv.) and diisopropylethylamine (0.053 ml, 1.0 equiv.) were added and the reaction mixtures were maintained for a further 7 h. After removal of the solvent, the residue was dissolved in $CHCl_3$, washed with H_2O and then continuously with aqueous Na_2SO_4. The $CHCl_3$ layer was dried over Na_2SO_4 and evaporated. The oily residue was washed with hexane-diethyl ether (4:1) three times and the remaining residue (crude material **2**) (302.8 mg) was purified by centrifugal partition chromatography ($CHCl_3$: CH_3OH: H_2O = 5:6:4, ascending mode), to give mixtures containing *N*-allyl-ACM (108.2 mg). The crude materials were passed through a Dowex 1 × 2, (chloride form, CH_3OH: H_2O = 1:4), and finally purified by silica gel column chromatography ($CHCl_3$:CH_3OH:H_2O = 10:1:0.1), to give pure *N*-allyl-ACM (71.0 mg, yield 26%) as an orange powder.

HRMS (ESI$^+$ mode): *m/z* 852.38267 (observed), *m/z* 852.38010 (calcd. for $C_{45}H_{58}NO_{15}^+$); ^{1}H-NMR of rhodosamine and D-ring moieties (chemical shift in p.p.m., splitting pattern, *J* in Hz) in $CDCl_3$: H-7 (5.12, d, 5.5), H-8a (2.15, d, 15.0), H-8b (2.58, dd, 5.5 and 15.0), 9-OH (4.76, br s), H-10 (4.06, s), H-13a (1.69, dq, 7.5 and 15.0), H-13b (1.76, dq, 7.5 and 15.0), H-14 (1.15, t, 7.5), -COOMe (3.67, s), H-1′ (5.78, br d, 2.0), H-2′a (overlapping at around 2.1 p.p.m.), H-2′b (overlapping at around 2.3 p.p.m.), H-3′ (5.08-5.14, m), H-4′ (4.44, br s), H-5′ (4.61, q, 7.0), H-6′ (1.36, d, 7.0). *Optical rotation*: $[\alpha]_D^{27}$ −1.7(*c* 0.1, $CHCl_3$) NMR table of *N*-allyl-ACM is presented in Table 1.

In vitro FTase assay

In vitro FTase assay was carried out according to the procedures previously described.[5] In brief, the standard reaction mixture of FTase contained the following components in a final volume of 60 µl:10 µg of partially purified FTase from human esophageal tumor EC17 cells, 10 µg of recombinant GST-H-Ras protein, 0.06 µM of (^{3}H)-farnesyl pyrophosphate (FPP) (596 GBq mmol^{-1}; New England Nuclear, Boston, MA, USA), 50 mM Tris–HCl (pH 7.5, Sigma, St Louis, MO, USA), 50 µM $ZnCl_2$ (Kanto Chemical Co., Tokyo, Japan), 4 mM $MgCl_2$ (Wako Pure Chemical Industries Ltd, Osaka, Japan) and 4 mM DTT (Wako). The reaction was initiated by the addition of enzyme and incubated for 1 h at 37 °C. The reaction was stopped by the addition of 0.5 ml of 1% sodium dodecyl sulfate (SDS, Wako) in MeOH and 0.5 ml of 30% trichloroacetic acid (TCA, Wako). The mixture was then filtered through a Whatman GF/C filter (GE Healthcare, Buckinghamshire, UK), washed with 5 ml of 6% TCA. The dried filter was finally placed in a liquid scintillation counter (Beckman Coulter, Inc., Miami, FL, USA). A blank value was determined in a parallel incubation with boiled enzymes and was subtracted before calculating percent inhibition.

Detection of H-Ras translocation to plasma membrane

Human epidermoid carcinoma A431 cells (1 × 10^6) were seeded in 10 cm dishes and cultured overnight. After the culture supernatant was replaced with DMEM (Nissui Pharmaceutical, Tokyo, Japan) supplemented with 0.2% calf serum, the cells were pretreated with drugs for 15 min and stimulated with 30 ngml^{-1} epidermal growth factor (EGF, Sigma). Following 24 h of incubation, cells were collected and resuspended in buffer A (20 mM Hepes (Sigma), pH 7.5, 10 mM KCl (Kanto Chemical), 1.5 mM $MgCl_2$, 1 mM EDTA (Kanto Chemical), 1 mM EGTA (Wako) and 1 mM DTT containing 250 mM sucrose (Sigma) and 1 mM phenylmethylsulfonyl fluoride (PMSF, Sigma). The cells were homogenized and unbroken cells were removed by centrifuging the homogenates at 1,000 × g for 10 min at 4°C. The supernatant was centrifuged at 100 000 × g for 1 h at 4 °C. The supernatant was removed and the pellets were lysed in radioimmunoprecipitation assay buffer buffer (25 mM Hepes, 1.5% Triton X-100 (Wako), 1% sodium deoxycholate (Wako), 0.1% SDS, 0.5 M NaCl (Wako), 5 mM EDTA, 50 mM NaF (Sigma), 0.1 mM sodium vanadate (Sigma) and 1 mM PMSF, pH 7.8) with sonication. The lysates were centrifuged at 100 000 × *g* for 15 min at 4 °C to give the plasma membrane fraction. The cells were also directly lysed in radioimmunoprecipitation assay buffer buffer with sonication, and the resultant samples were used as the total cell lysate. All samples were subjected to western blotting to detect H-Ras protein.

Transwell migration assay

Cell migration was assayed with a chemotaxis chamber (Becton Dickinson, Franklin Lakes, NJ, USA). A431 cells (7.5 × 10^4) suspended in DMEM supplemented with 0.2% calf serum were incubated in the upper chamber; the lower chamber contained DMEM supplemented with 0.2% calf serum in the presence or the absence of EGF (30 ngml^{-1}). Drugs were added to both chambers. Following 24 h of incubation, the filter was fixed with MeOH and stained with hematoxylin (Sigma). The cells attached to the lower side of the filter were counted.

RESULTS AND DISCUSSION

Screening for inhibitors of FTase

We evaluated the inhibitory activity of compounds against FTase in the project of the SCADS. SCADS is offering several biological activity evaluation of synthesized or isolated compounds for Japanese chemists. For the *in vitro* FTase assay, FTase was partially purified from human esophageal tumor EC17 cells and recombinant GST-H-Ras and (^{3}H)-FPP were used as the substrates. We firstly investigated the effect of compounds on FTase activity at the concentration of 10 µM. As a result, two compounds were found to have inhibitory activity against FTase. As shown in Figure 1, these are novel derivatives of ACM, and were named *N*-benzyl-ACM and *N*-allyl-ACM, respectively. ACM was discovered from a culture of *Streptomyces galilaeus*, and it showed potent antitumor activity.[6,7]

Effect of *N*-benzyl-ACM and *N*-allyl-ACM on FTase activity

In the next step, we examined the inhibitory activities of these ACM derivatives to give IC_{50} values. As shown in Figure 2, *N*-benzyl-ACM and *N*-allyl-ACM inhibit FTase activity in a dose-dependent manner, and the IC_{50} values of *N*-benzyl-ACM and *N*-allyl-ACM were 0.86 and 2.93 µM, respectively (Table 2). On the other hand, ACM did not inhibit FTase activity at a concentration of 10 µM in the process of the screening project of SCADS. Interestingly, neither the C-10 epimer of *N*-benzyl-ACM (10-epi-*N*-benzyl-ACM, see Supplementary Information) nor the C-10 epimer of *N*-allyl-ACM (10-epi-*N*-allyl-ACM, see Supplementary Information) showed an inhibitory effect against FTase activity at a concentration of 10 µM. These results indicated that both modification of the *N*-dimethyl group and the configuration of C-10 are critical for the inhibitory activity of *N*-benzyl-ACM and *N*-allyl-ACM toward FTase. Like FTase, geranylgeranyl transferase (GGTase) catalyzes the geranylgeranylation of proteins terminating with a CAAX motif, where X is restricted to leucine, isoleucine or phenylalanine. FTase and GGTase have been shown to be heterodimers that share a common α subunit with a different β subunit; therefore, we examined the effect of *N*-benzyl-ACM and *N*-allyl-ACM on the inhibitory activity against GGTase and

Table 1 ^{13}C- and ^{3}H-NMR data for N-benzyl-ACM and N-allyl-ACM

Position	δ_H	*mult.*		*J*	*Position*	δ_C
N-benzyl-ACM						
H-1	7.75	1H	dd	1.5Hz, 7.5Hz	C-1	120.1
H-2	7.64	1H	dd	7.5Hz, 8Hz	C-2	137.4
H-3	7.25	1H	dd	1.5Hz, 8Hz	C-3	124.7
					C-4	162.4 or 162.5
					C-4a	115.7
					C-5	192.7
					C-5a	114.4
					C-6	162.4 or 162.5
					C-6a	132.1 or 132.3
H-7	5.18	1H	d	5.5Hz	C-7	69.25 or 69.33
H-8a	2.20	1H	d	15Hz	C-8	36.5
H-8b	2.61	1H	dd	5.5Hz, 15Hz		
					C-9	70.4
H-10	4.12	1H	s		C-10	55.6
					C-10a	143.9
H-11	7.68	1H	s		C-11	121.2
					C-11a	132.1 or 132.3
					C-12	181.2
					C-12a	133.4
H-13a	1.69	1H	dq	7.5Hz, 15Hz	C-13	32.6
H-13b	1.79	1H	dq	7.5Hz, 15Hz		
H-14	1.15	3H	t	7.5Hz	C-14	6.98
H-1′	5.81	1H	brd	~2Hz	C-1′	99.0
H-2′a	2.02–2.17	1H	m		C-2′	26.5
H-2′b	2.35–2.45	1H	m			
H-3′	5.13	1H	brd	~14Hz	C-3′	67.2
H-4′	4.45	1H	brs		C-4′	76.1
H-5′	4.52–4.60	1H	m		C-5′	69.25 or 69.33
H-6′	1.38	3H	d	7Hz	C-6′	18.1
H-1″	5.31	1H	t	4Hz	C-1″	98.3
H-2″a,b	2.02–2.17	2H	m		C-2″	34.8
H-3″	4.05–4.13	1H	m		C-3″	66.0
H-4″	3.80	1H	t	3Hz	C-4″	78.5
H-5″	4.05–4.13	1H	m		C-5″	69.5
H-6″	1.27	3H	d	7Hz	C-6″	16.3
H-1‴	5.09	1H	t	6Hz	C-1‴	98.9
H-2‴a	2.02–2.17	1H	m		C-2‴	27.7
H-2‴b	2.35–2.45	1H	m			
H-3‴	2.44–2.53	2H	m		C-3‴	33.3
					C-4‴	209.6
H-5‴	4.44	1H	q	7Hz	C-5‴	71.7
H-6‴	1.31	3H	d	7Hz	C-6‴	14.8
4-OH	11.98	1H	s			
6-OH	12.78	1H	brs			
9-OH	4.57	1H	brs			
3″-OH	3.45	1H	d	6Hz		
COOMe	3.69	3H	s		COOMe	52.4
					COOMe	171.3
					Bzl-1	127.1
H-Bzl-2	7.41	2H	d	7.8Hz	Bzl-2	133.2
H-Bzl-3	7.19	2H	t	7.8Hz	Bzl-3	129.0
H-Bzl-4	7.32	1H	t	7.8Hz	Bzl-4	130.6
H-BzlCH_2a	4.60	1H	d	12.5Hz	Bzl-CH_2	66.6
H-BzlCH_2b	5.11	1H	d	12.5Hz		
N-Mea	3.08	3H	s		N-Mea	47.2
N-Meb	3.27	3H	s		N-Meb	46.6

Table 1 (Continued)

Position	δ_H	*mult.*		*J*	*Position*	δ_C
N-allyl-ACM						
H-1	7.68	1H	d	8Hz	C-1	120.1
H-2	7.60	1H	t	8Hz	C-2	137.5
H-3	7.20	1H	d	8Hz	C-3	124.8
					C-4	162.4 or 162.5
					C-4a	115.6
					C-5	181.1
					C-5a	114.3
					C-6	162.4 or 162.5
					C-6a	132.1 or 132.3
H-7	5.12	1H	d	5.5Hz	C-7	69.1
H-8a	2.15	1H	d	15Hz	C-8	36.4
H-8b	2.58	1H	dd	5.5Hz, 15Hz		
					C-9	70.3
H-10	4.06	1H	s		C-10	55.7
					C-10a	144.0
H-11	7.50	1H	s		C-11	121.2
					C-11a	132.1 or 132.3
					C-12	192.6
					C-12a	133.2
H-13a	1.69	1H	dq	7.5Hz, 15Hz	C-13	32.7
H-13b	1.76	1H	dq	7.5Hz, 15Hz		
H-14	1.15	3H	t	7.5Hz	C-14	7.1
H-1′	5.78	1H	brd	~2Hz	C-1′	98.9
H-2′a	2.03–2.16	1H	m		C-2′	26.2
H-2′b	2.22–2.36	1H	m			
H-3′	5.08–5.14	1H	m		C-3′	67.8
H-4′	4.44	1H	brs		C-4′	76.2
H-5′	4.61	1H	q	7Hz	C-5′	69.1
H-6′	1.36	3H	d	7Hz	C-6′	18.1
H-1″	5.28	1H	t	3.5Hz	C-1″	98.7
H-2″a,b	2.03–2.16	2H	m		C-2″	34.8
H-3″	4.06–4.13	1H	m		C-3″	66.0
H-4″	3.81	1H	t	2.5Hz	C-4″	78.6
H-5″	3.97–4.06	1H	m		C-5″	69.5
H-6″	1.28	3H	d	7Hz	C-6″	16.5
H-1‴	5.10	1H	t	6Hz	C-1‴	98.9
H-2‴a	2.03–2.16	1H	m		C-2‴	27.8
H-2‴b	2.38–2.54	1H	m			
H-3‴a,b	2.38–2.54	2H	m		C-3‴	33.3
					C-4‴	209.8
H-5‴	4.46	1H	q	7Hz	C-5‴	71.8
H-6‴	1.32	3H	d	7Hz	C-6‴	14.9
4-OH	11.93	1H	s			
6-OH	12.73	1H	brs			
9-OH	4.76	1H	brs			
3″-OH	3.5	1H	brd	6Hz		
COOMe	3.67	3H	s		COOMe	52.4
					COOMe	171.3
Allyl-1a	3.97–4.06	1H	m		C-Allyl-1	64.5
Allyl-1b	4.39	1H	dd	6Hz,13Hz		
Allyl-2	5.88–5.97	1H	m		C-Allyl-2	124.5
Allyl-3a	5.59	1H	d	17Hz	C-Allyl-3	129.8
Allyl-3b	5.62	1H	d	10Hz		
N-Mea	3.15	3H	s		NMea	47.6
N-Meb	3.24	3H	s		NMeb	47.4

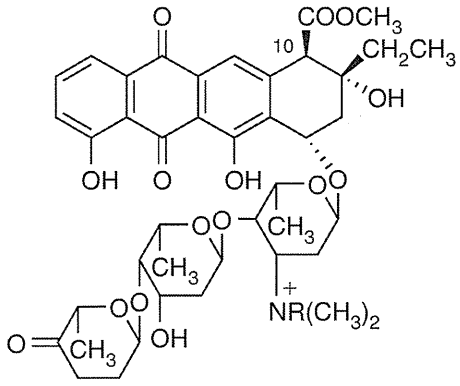

Aclacinomycin A (ACM); R=H
N-benzyl-ACM; R=$CH_2C_6H_5$
N-allyl-ACM; R=$CH_2CH{=}CH_2$

Figure 1 Structures of ACM derivatives.

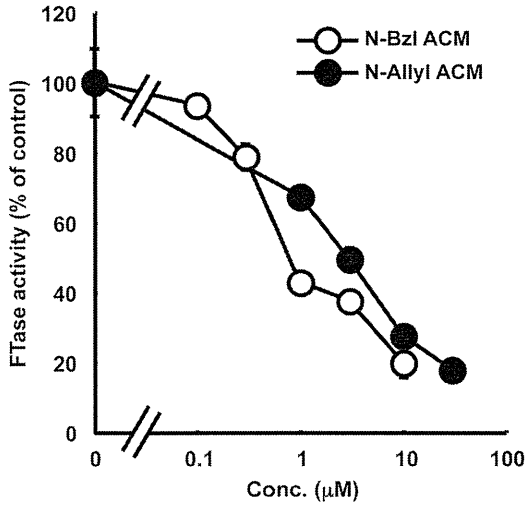

Figure 2 Effect of *N*-benzyl-ACM and *N*-allyl-ACM on FTase activity *in vitro*. Partially purified FTase from EC17 cells was incubated with (^{3}H)-FPP plus recombinant GST-H-Ras in the presence or absence of *N*-benzyl-ACM (*N*-Bzl-ACM) or *N*-allyl-ACM (*N*-Allyl-ACM). The reaction was terminated by the addition of TCA. The radioactivity of the TCA-insoluble fraction was measured. The results are the mean ± s.d. of two independent experiments.

Table 2 Effect of *N*-benzyl-ACM and *N*-allyl-ACM on FTase, GGTase and GGPP synthase activities *in vitro*, as well as cell migration and cell viability in A431 cells

	IC_{50} (μM)	
	N-benzyl-ACM	*N-allyl-ACM*
FTase	0.86	2.93
GGTase	100	>100
GGPP synthase	>100	>100
Cell migration	0.65	1.55
Cell viability (-EGF)	>10	>30
Cell viability (+EGF)[a]	9.09	22.0

[a]The concentration of EGF was 30 ng ml^{-1}.

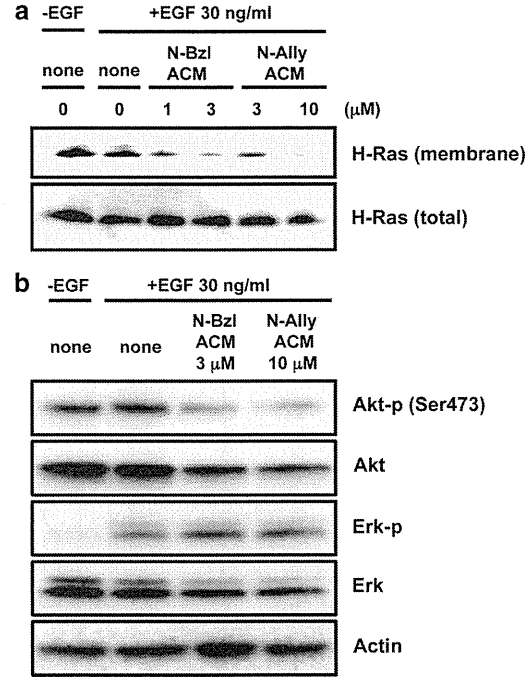

Figure 3 Effect of *N*-benzyl-ACM and *N*-allyl-ACM on H-Ras translocation, phosphorylation of Akt and Erk in A431 cells. (**a**, **b**) A431 cells were pretreated with drugs for 15 min and stimulated with EGF. Following 24 h of incubation, cells were collected and the membrane fraction was extracted (**a**) All samples were subjected to immunoblotting.

found that they failed to inhibit GGTase up to 100 μM. Geranylgeranyl pyrophosphate (GGPP) synthase is an enzyme that catalyzed the synthesis of GGPP from isopentenyl pyrophosphate and FPP; thus, because both FTase and GGPP synthase use FPP as a substrate, the effect of *N*-benzyl-ACM and *N*-allyl-ACM on GGPP synthase activity was examined. However, neither FTase inhibitor could inhibit GGPP synthase up to 100 μM (Table 2). So far, although several anthraquinones have been reported as FTase inhibitors,[8,9] none of the anthracycline family has been identified as an FTase inhibitor; thus, *N*-benzyl-ACM and *N*-allyl-ACM are the first examples in a series of the anthracycline family, demonstrating that the compounds inhibit FTase.

Effect of *N*-benzyl-ACM and *N*-allyl-ACM on localization of H-Ras

Because *N*-benzyl-ACM and *N*-allyl-ACM selectively inhibited FTase *in vitro*, next we examined whether these compounds could inhibit FTase in a cultured cell system. A431 cells were well-known EGF receptor-overexpressing cells that displayed a sufficient level of H-Ras protein[10] As shown in Figure 3a, the amount of H-Ras in the membrane fraction was not changed in the presence or absence of EGF; however, treatment of cells with *N*-benzyl-ACM and *N*-allyl-ACM reduced the amount of H-Ras in the membrane fraction. On the other hand, *N*-benzyl-ACM and *N*-allyl-ACM did not affect the geranylgeranylation of Rap1A in the same condition (data not shown). These results suggested that *N*-benzyl-ACM and *N*-allyl-ACM inhibited the membrane localization of H-Ras protein through the inhibition of FTase in A431 cells.

Effect of *N*-benzyl-ACM and *N*-allyl-ACM on PI3K signaling

The activation of H-Ras was reported to further activate the PI3K pathway.[11,12] Indeed, we previously reported that other FTase

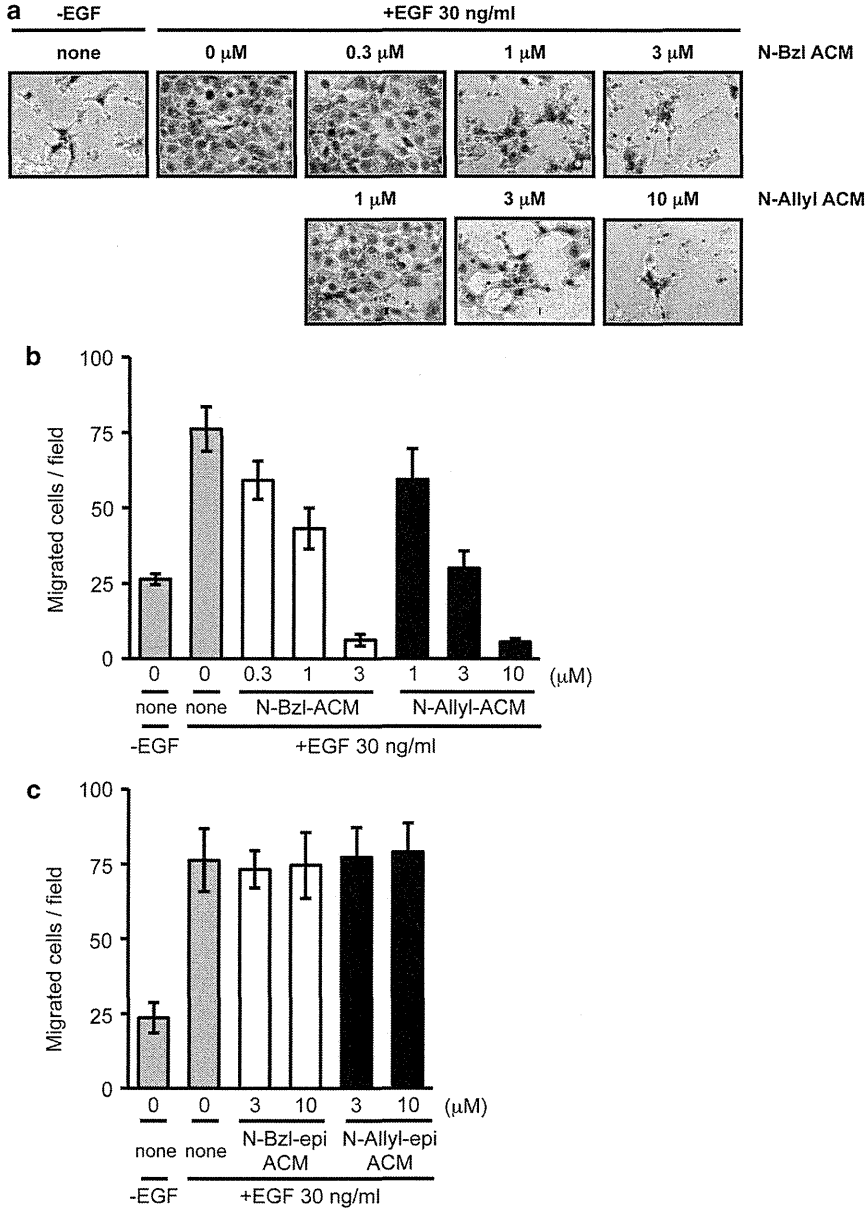

Figure 4 Effect of *N*-benzyl-ACM and *N*-allyl-ACM on EGF-induced cell migration in A431 cells. A431 cells suspended in DMEM supplemented with 0.2% calf serum were incubated in the upper chamber; the lower chamber contained DMEM supplemented with 0.2% calf serum in the presence or absence of EGF (30 ng ml^{-1}). Drugs were added to both chambers. After 24 h, the cells that migrated through the filter to the lower surface were photographed (**a**), and the number of migrated cells was counted (**b**, **c**). The results are the mean ± s.d. of five different fields.

inhibitors, moverastin A and B, inhibited the PI3K/Akt pathway but not the Raf/MEK/Erk pathway.[5] To confirm whether *N*-benzyl-ACM or *N*-allyl-ACM also could inhibit the PI3K pathway selectively, we examined the effect of these compounds on the phosphorylation of Akt or Erk in A431 cells. As shown in Figure 3b, the phosphorylation of Akt (Ser473) was significantly decreased in the presence of either *N*-benzyl-ACM or *N*-allyl-ACM, whereas these compounds did not affect the phosphorylation level of Erk. These results suggested that *N*-benzyl-ACM and *N*-allyl-ACM inhibited PI3K activation through the suppression of H-Ras farnesylation.

Effect of *N*-benzyl-ACM and *N*-allyl-ACM on cell migration

Since the activation of H-Ras through the farnesylation by FTase was involved in cell migration,[5] we examined the effect of N-benzyl-ACM or *N*-allyl-ACM on EGF-induced cell migration in A431 cells. As a result, *N*-benzyl-ACM or *N*-allyl-ACM inhibited EGF-induced cell migration in a dose-dependent manner (Figures 4a, b). These inhibitory effects were not due to the toxic effect of the drugs because their IC_{50} values for A431 cell viability were at least seven times higher than those for cell migration (Table 2). Importantly, the dose of *N*-benzyl-ACM or *N*-allyl-ACM required to inhibit cell migration was consistent with that for inhibition of the membrane localization of H-Ras. Moreover, according to the inhibitory activity against FTase, the IC_{50} value for the cell migration of *N*-benzyl-ACM was lower than that of *N*-allyl-ACM (Table 2). Neither 10-epi-*N*-benzyl-ACM nor 10-epi-*N*-allyl-ACM, which failed to inhibit FTase, suppressed EGF-induced migration of A431 cells (Figure 4c). Taken together, these findings suggest that *N*-benzyl-ACM and *N*-allyl-ACM inhibited